Morphology Evolution and Anisotropic Phase Formation of the Maleated Polyethylene−Layered Silicate Nanocomposites

ARTICLE *in* MACROMOLECULES · MAY 2002

Impact Factor: 5.8 · DOI: 10.1021/ma011770d

5 AUTHORS, INCLUDING:

Chong Min Koo
Korea Institute of Science and Technology
100 PUBLICATIONS **1,581** CITATIONS
SEE PROFILE

Sang Ouk Kim
Korea Advanced Institute of Science and Tec…
163 PUBLICATIONS **6,838** CITATIONS
SEE PROFILE

KiHyun Kim
Korea University
140 PUBLICATIONS **1,024** CITATIONS
SEE PROFILE

Morphology Evolution and Anisotropic Phase Formation of the Maleated Polyethylene-Layered Silicate Nanocomposites

Chong Min Koo, Hyeong Taek Ham, Sang Ouk Kim,† Ki Hyun Wang, and In Jae Chung*

Department of Chemical and Biomolecular Engineering, Korea Advanced Institute of Science and Technology, 373-1, Kusong-dong, Yusong-gu, Taejon 305-701, South Korea

Dae-Cheol Kim and Wang-Cheol Zin

Department of Material Science and Engineering, Pohang University of Science and Technology, San 31, Hyoja-dong, Nam-gu, Pohang, Kyoungpook 790-784, South Korea

Received October 11, 2001

ABSTRACT: Morphology evolution and anisotropic phase formation of the maleated polyethylene-layered silicate nanocomposites are investigated by using synchrotron small-angle X-ray scattering (SAXS), transmission electron microscopy (TEM), and polarized optical microscopy (POM). Despite favorable compatibility between polymer and organically modified layered silicates, the final morphology of the nanocomposite evolves via four stages: disordered exfoliation, ordered exfoliation, dual morphologies of intercalation and exfoliation, and intercalation in sequence with the content of silicate. The formation of the ordered exfoliation state is attributed to the steric interaction between anisotropic silicate plates. Particularly, the transition from exfoliation to intercalation provides us with the significant clue that the interaction between layer silicates gets dominant when the distance between them is smaller than a certain value. It is found that the silicate layers need larger layer spacing than 9 nm to avoid the attractive interaction between adjacent silicate layers and to keep the exfoliation state in this nanocomposite system. Additionally, the nanocomposite shows the optical anisotropy above 12 vol % clay due to the ordering of silicate layers. The optical anisotropy becomes stronger with the content of silicate.

Introduction

Polymer-layered silicate (PLS) nanocomposites have attracted great attention due to their academic and industrial importance. They have shown dramatic improvements in mechanical, thermal, and barrier properties with a small amount of inorganic layered silicate.[1−9] Moreover, they can provide good model system for the studies of the phase behavior of a polymer−nanoparticle mixture[19−30] as well as the polymer chain dynamics in the confined geometry.[10−18]

From the structural point of view, PLS nanocomposites can be classified into *intercalated* and *exfoliated*. *Intercalated* state is termed for the nanocomposite structure where the extended polymer chains are inserted into the gallery space between the individual silicate layers, preserving the well-ordered multilayer structures of silicate. *Exfoliated* state implies the structure where the interaction between the individual silicate layers no longer exists. An ideal exfoliated state, where the silicate plates are homogeneously dispersed in the polymer matrix, is one of the ultimate aims in the fabrication of PLS nanocomposite. However, it is well-known that because it is hard to exfoliate the tightly stacked silicate plates with van der Waals gap,[8−10] the favorable interaction between silicate and matrix polymer is necessary for the exfoliation.[26−30]

Recently, Balazs and co-workers conducted a simulation based on analytical self-consistent theory (SCF), considering the interactions among polymer, silicate, and organic modifier. They predicted that the nanocomposite with monodisperse silicate plates would form various mesophases depending on the interactions and the concentration of silicate.[26−30] To the best of our knowledge, however, there is no experimental research dealing with the structural change with the content of silicate filler, which is mainly due to the difficulty of preparing highly loaded nanocomposites with homogeneous dispersion of silicate plates. Because the natural silicate plates have the broad distribution of size and shape, it can be expected that the structural evolution of the real nanocomposite system should be quite different from the ideal monodisperse case.

In this work, maleated polyethylene (MAPE)/organically modified montmorillonite (20A) nanocomposite is used as a model system to investigate the structural evolution of nanocomposite with the content of natural silicate filler. To overcome the limitation in processing, the extremely slow relaxation, and high elasticity of highly loaded nanocomposites, the maleated polyethylene with a low molecular weight is used. With this approach homogeneous nanocomposites are successfully prepared up to the highest silicate content of 36 vol %.

Experimental Section

Materials. Maleated polyethylene (MAPE) was obtained by Aldrich Co. The basic characteristics of MAPE used in this study are summarized in Table 1. Organophilic montmorillonite (Cloisite 20A, abbreviation: 20A) used in this study was purchased from Southern Clay. 20A is known to be ion-exchanged with dimethyl dehydrogenated tallow ammonium ions. It was found that 20A contains organic modifier of about 30 wt % by the measurement of TGA. The specific gravity of

† Current address: Department of Chemical Engineering, University of Wisconsin−Madison, 2020 Engineering Hall, 1415 Engineering Drive, Madison, WI 53706-1691.

* Corresponding author: e-mail chung@kaist.ac.kr; Tel +82-42-869-3916; FAX +82-42-869-3910.

10.1021/ma011770d CCC: $22.00
Published on Web 05/22/2002

Table 1. Characterization of Maleated Polyethylene (MAPE)

	M_w[a]	PDI (M_w/M_n)[a]	T_m (°C)[b]	MA content[c] (wt %)
MAPE	9300	2.1	99.3	3.0

[a] Measured by GPC. [b] Measured by DSC at the 10 °C/min heating. [c] Measured by elemental analysis.

20A measured by a pycnometer was 1.8 g/mL. Nanocomposites were prepared by the melt intercalation method. MAPE was mechanically mixed with 20A for 20 min in a brabender mixer at 160 °C. For all the content of silicate extruded fiber samples were prepared to verify the effect of the preparation history on the structure formation. The extrusion was conducted with a capillary viscometer (Rosand RH5) at a high shear rate of 1000 s^{-1}.

Characterization. The periodic structure of silicate layers in the MAPE/20A nanocomposite was evaluated by the synchrotron SAXS with point focusing (0.2 × 0.2 mm) at the 4C2 beamline in the Pohang Accelerator Laboratory (PAL), Korea, which consisted of a 2 GeV LINAC accelerator, storage ring, Si (111) double crystal monochromator, and ion chambers. A beam path was maintained under a vacuum to reduce air scattering, and tungsten foil (50 μm) was used for primary beam protection. A small amount of nanocomposite and the bundle of the arranged fibers were sealed between Kapton film windows (7 μm thick) to preserve the fixture. One-dimensional (1-D) SAXS patterns were obtained from a diode-array position-sensitive detector with 2048 pixels. The measured intensity was corrected for background scattering, detector noise, and absorption by the sample. Two-dimensional (2-D) SAXS patterns were recorded in imaging plates with 2000 × 4000 pixels and read out with scanner (MAC Science). The distance between the sample and detector (or imaging plate) was 600 mm. The morphology of MAPE/20A nanocomposite was observed by TEM (Philips CM-20 transmission electron microscope) after cryogenic ultra-microtoming (RMC MT7000). The birefringence was studied by a polarized optical microscope (POM, A Leitz, model Laborlux 12 Pols) coupled with a Mettler FP-2 hot stage at 160 °C.

Results and Discussion

Morphology Evolution of the Nanocomposites. In this work, the periodic structure of silicate layers in the nanocomposite was quantified through the SAXS experiments. To determine the exact peak positions in the SAXS patterns, a deconvolution procedure was performed. Experimental curves can be expressed as the sum of the Gaussian function and the first-order exponential decay function:

$$I(q) = I_{\text{Gaussian}} + I_{\text{Guinier}} \tag{1}$$

$$I(q) = \sum_i \frac{a_i}{w_i\sqrt{\pi/2}} \exp\left[-\frac{2(q-q_i)^2}{w_i^2}\right] + b + c\exp\left[-\frac{q}{t}\right] \tag{2}$$

where Bragg diffraction satisfies well the Gaussian function, and the exponential decay function is most suitable for baseline fit. Although the Guinier scattering function is appropriate in a dilute particulate system, the first-order exponential decay function was well fitted in these nanocomposites. Figure 1 shows two examples of scattering patterns of the nanocomposites with 15 and 24 vol % silicate content. Bragg reflections can be obtained by the nonlinear fit on the basis of eq 2. The nanocomposite with 15 vol % silicate in Figure 1a shows two reflection peaks where the peak position ratios are almost 1:2. This indicates that these peaks are originated from the same periodic structure of the silicate layers.[9,35] Figure 1b shows the SAXS pattern of the nanocomposite with 24 vol % silicate. The two reflection peaks are separated, and the intensity of the second peak is more intense than that of first peak. Also, these peaks do not satisfy the multiple relationships. It indicates that two peaks are originated from the different periodic structures of the silicate layers. These double-plane peaks are observed for the nanocomposite with 21 and 24 vol % silicate content. The peak position of all nanocomposites was determined by this deconvolution procedure, and the obtained fitting parameters are shown in Figure 1.

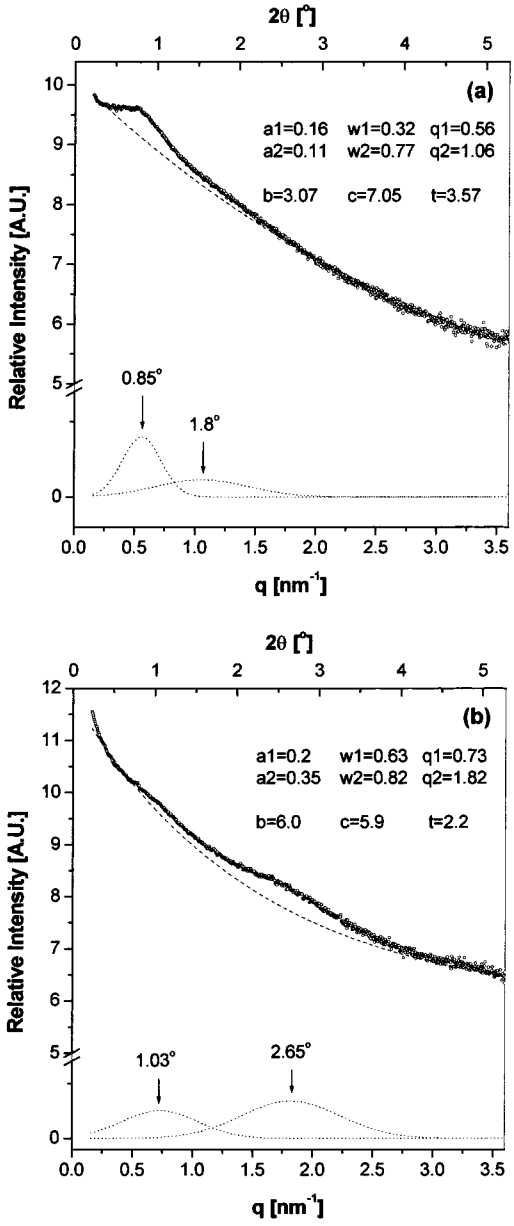

Figure 1. SAXS patterns for the nanocomposites with 15 and 24 vol % silicate. The line represents the best fit summarizing contributions from the baseline (dashed line) and the Bragg reflections (dotted line).

Figure 2a,b shows the SAXS patterns of as-mixed and extruded nanocomposites to examine the effect of preparation history. The scattered intensities of the extruded nanocomposite were recorded in the vertical direction to the shear direction. Although the extrusion process enhances intensity and sharpness of the (001) reflection

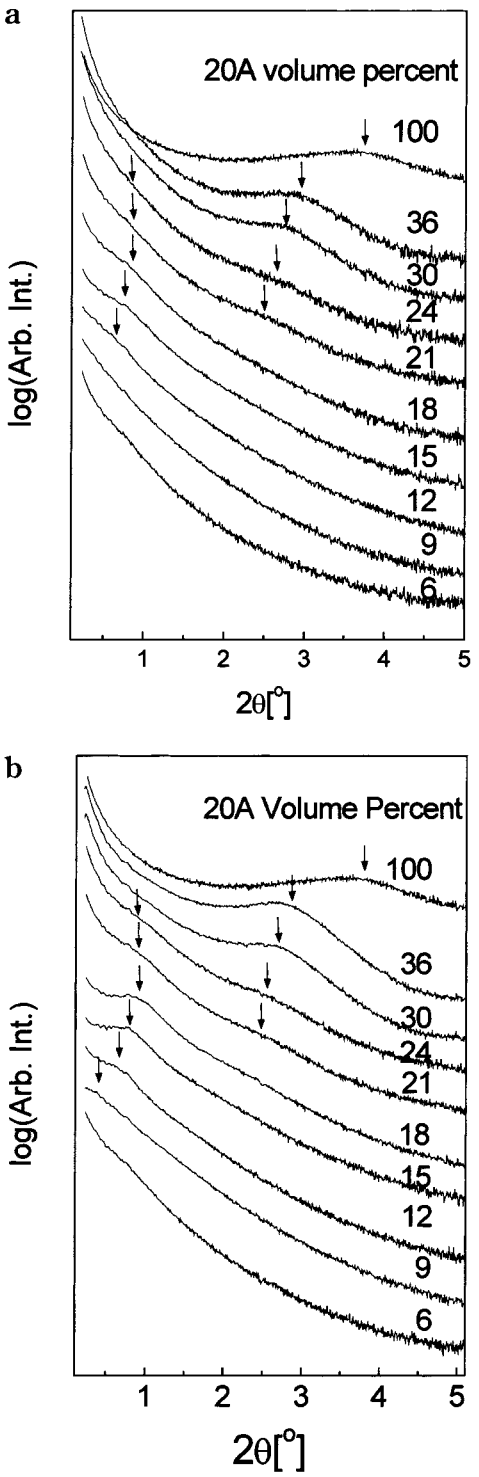

Figure 2. SAXS patterns of (a) as-mixed and (b) extruded nanocomposites to examine the effect of preparation history.

peak slightly, the SAXS patterns of both samples are intrinsically same except for a nanocomposite with 9 vol % silicate. The weak and broad (001) reflection peak around 0.5° appears only after the extrusion, which indicates that the ordered layer structure can be induced by a high shear flow at this content.[31]

The measured *d* spacings are plotted as a function of the content of silicate in Figure 3. The shear-induced reflection peak of 9 vol % nanocomposite is marked with a triangle symbol. The solid line is the *d* spacing evaluated with Vincent and co-workers' equation,[32] which is established according to Brown's description,[33]

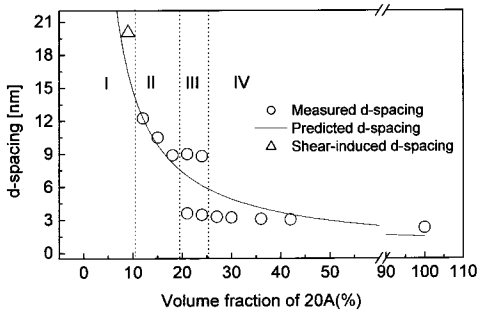

Figure 3. Measured and predicted *d* spacings of the nanocomposites as a function of the content of silicate. Open circle symbol indicates the *d* spacing calculated from experimental SAXS data. The shear-induced reflection peak of 9 vol % nanocomposite is marked with the triangle symbol. The solid line is the layer spacing fitted with the Vincent and co-workers' equation.[32]

where disk-shaped particles have an alternative parallel arrangement.

$$(2R + b)^2(H + a) = \frac{\pi R^2 H}{\phi} \tag{3}$$

ϕ is the volume fraction of the 20A particles; R and H are the radius and the thickness of the disk, respectively. a and b are the separation gap between adjacent disks (face-to-face distance) and a lateral separation (edge-to-edge distance), respectively. Thus, the *d* spacing of the silicate layers corresponds to the sum of H and a. The parameters $2R$ and b are 140 and 30 nm, respectively, which are evaluated from the investigation of TEM images. Since 20A is the montmorillonite coated with organic modifier, we considered H as the effective thickness of 2.3 nm (basal spacing of 20A) instead of the thickness of the pure clay platelet 0.95 nm, to simplify tertiary systems consisting of MAPE, modifier, and pure clay into secondary system consisting of MAPE and 20A. The predicted solid line agrees quite well with the measured *d* spacings of nanocomposites up to the silicate content of 18 vol %. The good consistency between experimental data and the fitted line indicates that the silicate layers are quite homogeneously distributed over the whole range of silicate concentration. The deviation above 21 vol % is due to the structural change of nanocomposite, which is discussed below.

The *d* spacing of silicate layers in MAPE/20A nanocomposites varies via four stages (I−IV) as a function of content of silicate. In the lowest content range up to 9 vol % (stage I), the periodicity of the silicate layers is not observed without the extrusion process, which implies that the silicate plates have the disordered and exfoliated structure in polymer matrix. In the content range between 12 and 18 vol % (stage II), each nanocomposite shows a single plane peak, corresponding to the (001) reflection of basal spacing. The layer spacing gradually decreases following the prediction by eq 3, which implies that the nanocomposites have the ideally exfoliated morphology with homogeneous dispersion of silicate plates. These results support that the periodicity of the silicate layers is originated from the steric interaction between silicate layers having anisotropic shape, as predicted by Balazs and co-workers.[26−30] In the content range of 21−24 vol % silicate (stage III), the nanocomposite shows a distinct dual structure, indicating the coexistence of exfoliation and intercalation. The *d* spacing of the higher angle peak is below approxi-

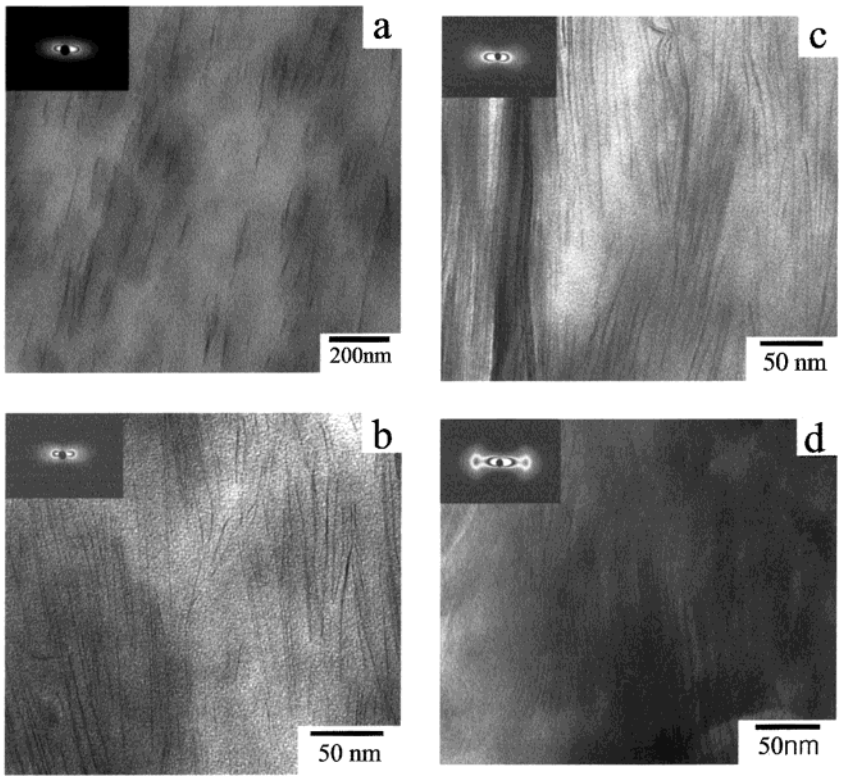

Figure 4. Transmission electron micrographs of the MAPE/20A nanocomposites with clay concentration of (a) 6, (b) 18, (c) 24, and (d) 36 vol % silicate. Insets show the 2-D SAXS patterns of these specimens. The nanocomposite fiber is laid in the meridian in the images. The flow direction corresponds to the meridian direction.

mately 3.5 nm, which corresponds to the layer spacing between silicate plates with two or three polyethylene chain inside the gallery. The peak corresponding to the exfoliated silicate plates persists, but its *d* spacing deviates from the prediction of eq 3. The relative intensity of the peak corresponding to the intercalated portion is higher at the higher content of silicate of 24 vol %, which is a typical behavior at a transition region. The present result clearly demonstrates that the attractive interaction between silicate plates becomes dominant at a critical content of silicate even with the quite favorable interaction between silicate plates and polymer chain. In this particular nanocomposite system, the critical length for this transition is 9 nm approximately. Above 27 vol % of silicate (stage IV), only one plane peak is observed. It indicates the intercalated structure of silicate layers. The layer spacing also gradually deceases with the concentration of silicate.

A typical transmission electron micrograph of MAPE/20A nanocomposite at each structural stage is shown in Figure 4. The extruded nanocomposites were sliced in the parallel direction with shear flow using a cryogenic ultra-microtome at −120 °C. Insets show the corresponding 2-D SAXS pattern. The flow direction is parallel to the meridian in images. Silicate plates are shown as dark lines in the images. They show a broad distribution of diameter in the range between 30 and 300 nm and have the uniform thickness of 1 nm, which is a typical property of a natural smectite. Additionally, all insets in Figure 4 show the strongly anisotropic intensity distribution on the equator, indicating that the silicate layers are highly oriented in the flow direction. Figure 4a shows the transmission electron micrograph of the nanocomposite with 6 vol % silicate (stage I). One can observe that individual silicate layer is well dispersed in the polymer matrix, and it agrees well with the result of SAXS experiments. They are aligned quite well in the meridian direction, that is, in the applied shear direction on the extrusion process. In the inset, one can see a reflection around the beam stopper, which is a typical 2-D SAXS pattern of the exfoliated nanocomposite.[34−36] As can be expected with the 1-D SAXS result in Figure 2a, silicate plates orient randomly in the as-mixed nanocomposite. Figure 4b shows the transmission electron micrograph of the nanocomposite fiber with 18 vol % silicate (stage II). The silicate layers are well dispersed in the polymer matrix again. The fairly close distance between adjacent silicate layers and their parallel arrangement support that the nanocomposite with 18 vol % silicate has the ordered and exfoliated morphology. The mean layer spacing measured from TEM is about 9.0 nm, which is comparable to that of 8.9 nm obtained from SAXS. Figure 4c shows the photograph of the nanocomposite fiber with 24 vol % silicate (stage III). One can observe a tightly stacked layer structure as well as a quite loosely aligned layer structure. The tightly stacked layer structure is a typical intercalation structure, where it keeps the narrower layer spacing than 3.5 nm, whereas some exfoliated silicate plates remain, keeping the wider layer spacing above 9 nm, which agrees well with the results of SAXS experiments. In the inset, the nanocomposite with 24 vol % silicate has a pair of reflections on the equator near the beam stopper. The intensity maximum is observed in the inner reflection, and the additional weak outer reflection for the intercalated structure is also seen.[34−36] Figure 4d shows the photograph of the nanocomposite fiber with 36 vol % silicate (stage IV). Only the tightly stacked layer structure, a typical intercalated morphology, is seen over the whole sample. The mean layer spacing is consistent with the value of 3.1 nm in SAXS. In the inset, we can see a pair of reflections on

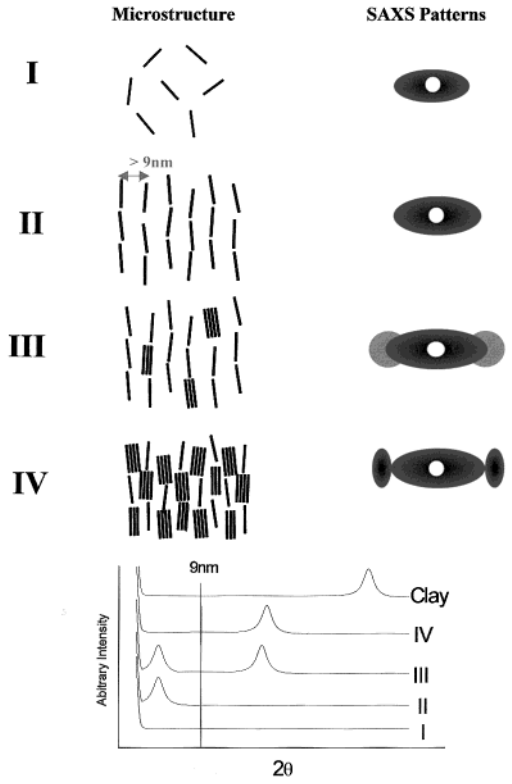

Figure 5. Schematic representation of the evolution of the microstructure and their SAXS patterns as a function of the concentration of the silicate.

the equator near the beam stopper. However, there is no intensity maximum in the inner reflection. The intensity maximum of the outer reflection produces (001) plane reflection of the silicates.

In Figure 5 the evolution of the microstructure is schematically summarized with the SAXS patterns as a function of silicate content. The oriented state is seen well in the 2D-SAXS patterns. Stage I indicates the disordered and exfoliated state. The individual silicate layer is randomly distributed because individual layers could keep the interlayer distance as far as they could not interact sterically. Nevertheless, the artificially oriented extrudate would show the layer spacing if the interlayer distance exists within the detectable range. Stage II indicates the ordered and exfoliated state. The orientation of each silicate plate is affected by adjacent ones because the interlayer distance is quite smaller than the diameter of plate. It should be noted that the ordering of stage II is not due to particular attraction or repulsion but due to the steric interaction of silicate layers with a large aspect ratio,[19−30] which is supported by the result that the relationship between the layer spacing and the concentration of silicates presented in eq 3 is satisfied well in this stage. Stage II has a similar 2-D SAXS pattern and a different 1-D SAXS pattern when compared with stage I. The mean interlayer distance remains above 9 nm up to stage II. Stage III shows the dual morphologies of exfoliation and intercalation. The layer spacing does not follow the predicted line but transits abruptly in this stage. It implies that there is a critical distance between silicate plates (about 9 nm in this nanocomposite), below which the attractive interaction (van der Waals force) between silicate plates overwhelms the favorable interaction between silicate plate and polymer chain. The SAXS pattern shows a pair of reflections on the equator near the beam stopper in 2D-SAXS and the dual plane peaks in 1D-SAXS. Stage IV shows one peak in 1D-SAXS. The intercalation is the dominant state. Because of the high content of silicate, silicate plates cannot keep the enough distance between them for the exfoliation. SAXS pattern shows a pair of reflections on the equator in 2D-SAXS.

Anisotropic Phase Formation of the Nanocomposite. Figure 6 shows the polarized optical micrographs of the extruded nanocomposite fibers with a diameter of 1 mm at 160 °C, which is above the melting temperature of MAPE. The extruded fibers show the darkness in the polarized optical microscope up to 6 vol % silicate. At 9 vol % of silicate, birefringence starts to appear. Optical anisotropy becomes stronger with the content of silicate filler. It is clear that the optical anisotropy must be originated from the ordering of the silicate plates in the flexible polymer, MAPE.

Figure 7a−c shows the polarized optical micrographs of the as-mixed nanocomposites. Figure 7d shows the polarized optical micrograph of the extruded nanocomposite fiber with 18 vol % silicate. The samples on the slide glass were squeezed very slowly with a cover glass to minimize the history of sample preparation at 160 °C. The unextruded nanocomposites show the optical anisotropy not from 9 vol % but from 12 vol %. The nanocomposite containing 9 vol % silicate shows clear

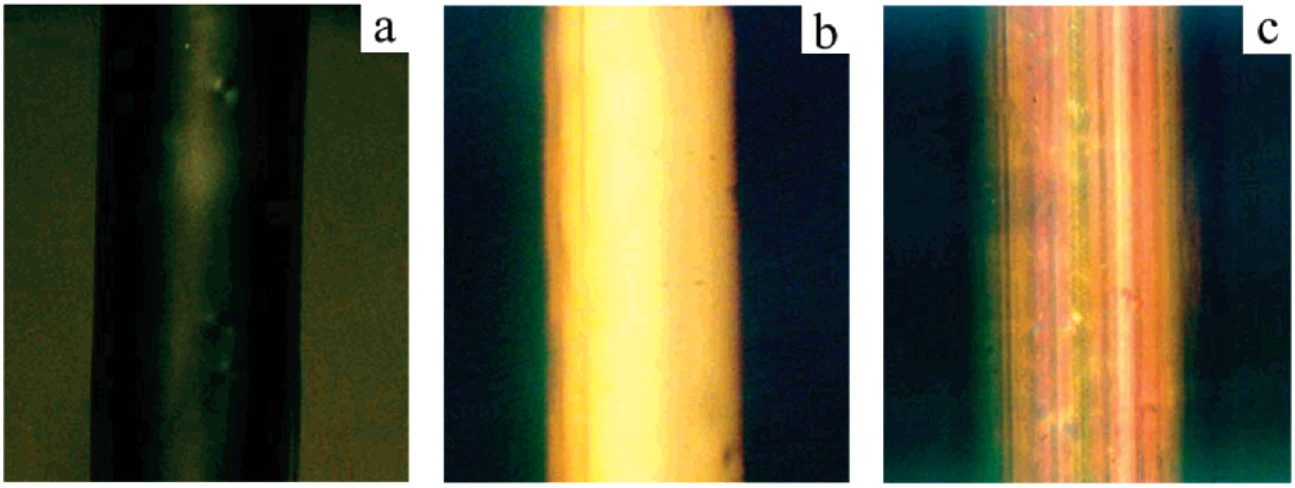

Figure 6. Polarized optical micrographs of the nanocomposite fibers with the concentration of (a) 6, (b) 9, and (c) 15 vol % silicate.

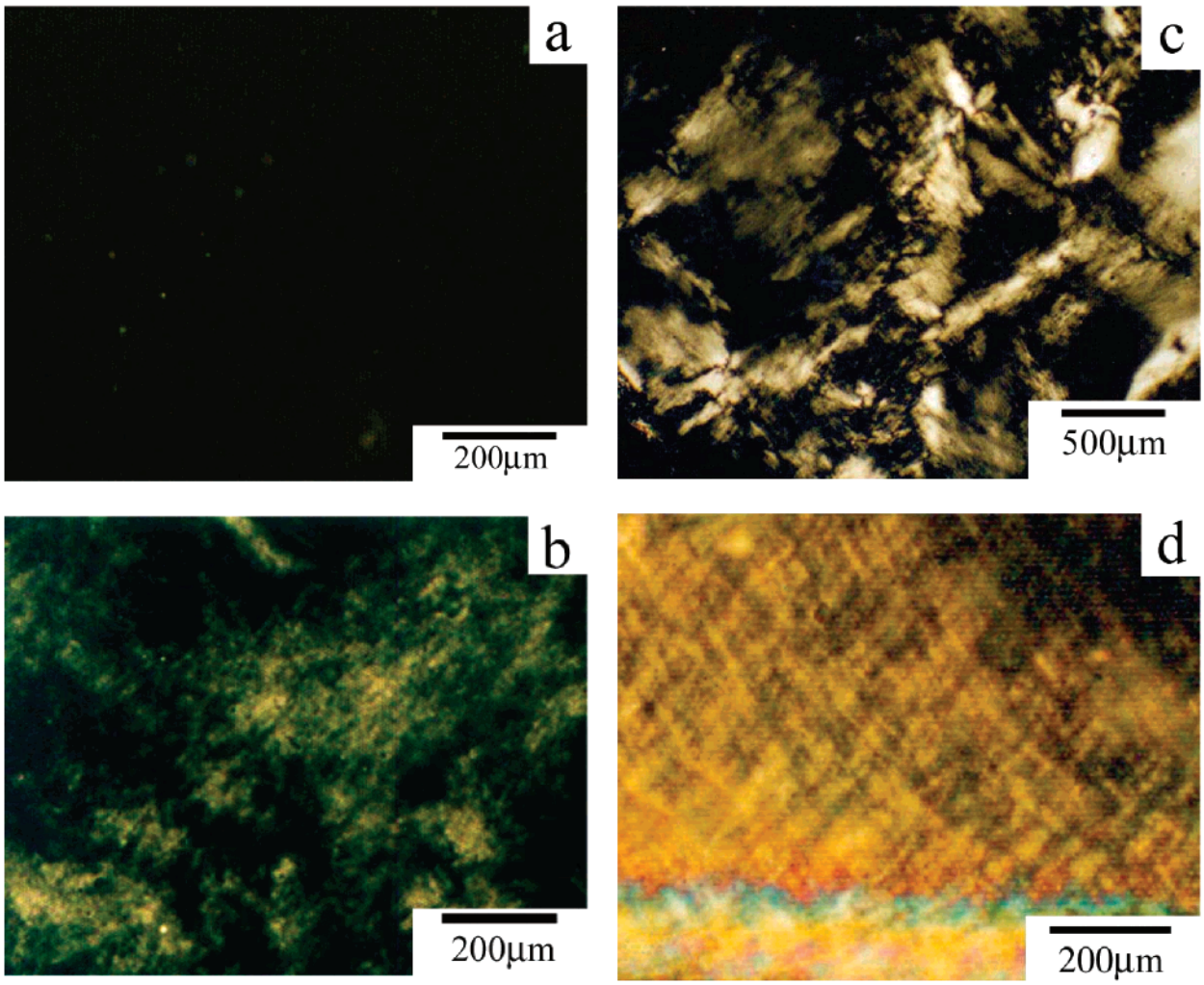

Figure 7. Polarized optical micrographs of the as-mixed MAPE/20A nanocomposite with concentration of (a) 9, (b) 12, and (c) 18 vol % silicate and the extruded nanocomposite fiber with concentration of (d) 18 vol % silicate. Samples on the slide glass were squeezed very slowly with a cover glass to minimize the history of sample preparation at 160 °C. Especially, the extrudate was hardly squeezed to keep the sheared state.

birefringence in the extruded state, not in the unextruded state. It indicates that the nanocomposites show a shear-induced optical anisotropy. Also, the extruded nanocomposite fiber with 18 vol % silicate shows a more brightened and colorful texture than the unextruded one.

Conclusion

Morphology evolution and anisotropic phase formation of the maleated polyethylene-layered silicate nanocomposites were investigated. The microstructure of the nanocomposites evolved via four stages as the concentration of silicate increases. In stage I with lower concentration of silicate than 9 vol %, the nanocomposites had the disordered and exfoliated morphology. In stage II with the intermediate concentration range of 12−18 vol % silicate, the nanocomposites had the ordered and exfoliated structure due to the ordering of silicate plates induced by steric interaction. In stage III with the concentration range of 21−24 vol % silicate, the intercalation and the exfoliation coexist and transition between them is not continuous. In stage IV with the concentration range above 27 vol % silicate, intercalation morphology was dominant. The existence of dual morphologies in stage III clearly demonstrates the effect of an attractive interaction between adjacent layers on the morphology evolution as well as the range of the attractive interaction of 9 nm in this nanocomposite. The ordering of the silicate layers in the nanocomposite induced the optical anisotropy. The optical anisotropy started to appear at the silicate content of 12 vol % and became stronger as the content of silicate increases.

Acknowledgment. This work was supported by the Brain Korea 21 program and the Center for Advanced Functional Polymers in Korea Advanced Institute of Science and Technology. We thank Samsung General Chemicals for allowing the use of the cryogenic ultramicrotome.

References and Notes

(1) Kojima, Y.; Usuki, A.; Kawasumi, M.; Okada, A.; Fukushima, Y.; Kurauchi, T.; Kamigaito, O. *J. Mater. Res.* **1993**, *8*, 1185.
(2) Kojima, Y.; Usuki, A.; Kawasumi, M.; Okada, A.; Kurauchi, T.; Kamigaito, O. *J. Appl. Polym. Sci.* **1993**, *8*, 1185.
(3) Kawasumi, M.; Hasegawa, N.; Kato, M.; Usuki, A.; Okada, A. *Macromolecules* **1997**, *30*, 6333.
(4) Vaia, R. A.; Vasudevan, S.; Krawiec, W.; Scanlon, S. G.; Giannelis, E. P. *Adv. Mater.* **1995**, *7*, 154.
(5) Giannelis, E. P. *Adv. Mater.* **1996**, *8*, 29.
(6) Choi, M. H.; Chung, I. J.; Lee, J. D. *Chem. Mater.* **2000**, *12*, 2977.

(7) Wang, K. H.; Choi, M. H.; Koo, C. M.; Chung, I. J. *Polymer* **2001**, *42*, 9819.
(8) LeBaron, P. C.; Wang, Z.; Pinnavaia, T. J. *Appl. Clay Sci.* **1999**, *15*, 11.
(9) Alexandre, M.; Dubois, P. *Mater. Sci. Eng.* **2000**, *28*, 1.
(10) Vaia, R. A.; Jandt, K. D.; Kramer, E. J.; Giannelis, E. P. *Macromolecules* **1995**, *28*, 8080.
(11) Hackett, E.; Manias, E.; Giannelis, E. P. *Chem. Mater.* **2000**, *12*, 2161.
(12) Bujdak, J.; Hackett, E.; Giannelis, E. P. *Chem. Mater.* **2000**, *12*, 2168.
(13) Vaia, R. A.; Sauer, B. B.; Tse, O. K.; Giannelis, E. P. *J. Polym. Sci.* **1997**, *35*, 59.
(14) Krishnamoorti, R.; Vaia, R. A.; Giannelis, E. P. *Chem. Mater.* **1996**, *8*, 1728.
(15) Krishnamoorti, R.; Vaia, R. A.; Giannelis, E. P. *Macromolecules* **1997**, *30*, 4097.
(16) Vaia, R. A.; Giannelis, E. P. *Macromolecules* **1997**, *30*, 8000.
(17) Lim, Y. T.; Park, O. O. *Macromol. Rapid Commun.* **2000**, *21*, 231.
(18) Lim, Y. T.; Park, O. O. *Rheol. Acta* **2001**, *40*, 220.
(19) Onsager, L. *Ann. N. Y. Acad. Sci.* **1949**, *51*, 627.
(20) Langmuir, I. *J. Chem. Phys.* **1938**, *6*, 873.
(21) Davidson, P.; Batail, P.; Gabriel, J. C. P.; Livage, J.; Sanchez, C.; Bourgaux, C. *Prog. Polym. Sci.* **1997**, *22*, 913.
(22) Gabriel, J. C. P.; Davidson, P. *Adv. Mater.* **2000**, *12*, 9.
(23) Gabriel, J. C. P.; Sanchez, C.; Davidson, P. *J. Phys. Chem.* **1996**, *100*, 11139.
(24) van der Kooij, F. M.; Kassapidou, K.; Lekkerkerker, H. N. W. *Nature (London)* **2000**, *406*, 868.
(25) Lekkerkerker, H. N. W.; Stroobants, A. *Nature (London)* **1998**, *393*, 305.
(26) Lyatskaya, Y.; Balazs, A. C. *Macromolecules* **1998**, *31*, 6676.
(27) Balazs, A. C.; Singh, C.; Zhulina, E.; Lyatskaya, Y. *Acc. Chem. Res.* **1999**, *32*, 651.
(28) Ginzburg, V. V.; Balazs, A. C. *Macromolecules* **1999**, *32*, 5681.
(29) Ginzburg, V. V.; Singh, C.; Balazs, A. C. *Macromolecules* **2000**, *33*, 1089.
(30) Ginzburg, V. V.; Balazs, A. C. *Adv. Mater.* **2000**, *12*, 1805.
(31) Chen, G.; Liu, S.; Zhang, S.; Qi, Z. *Macromol. Rapid Commun.* **2000**, *21*, 746.
(32) Saunders, J. M.; Goodwin, J. W.; Richardson, R. M.; Vincent, R. *J. Phys. Chem. B* **1999**, *103*, 9211.
(33) Brown, A. B. D.; Clarke, S. M.; Bennie, A. R. *Langmuir* **1998**, *14*, 3129.
(34) Ogata, N.; Kawakage, S.; Ogihara, T. *J. Appl. Polym. Sci.* **1997**, *66*, 573.
(35) Jimenez, G.; Ogata, N.; Kawai, H.; Ogihara, T. *J. Appl. Polym. Sci.* **1997**, *64*, 2211.
(36) Kojima, Y.; Usuki, A.; Kawasumi, M.; Okada, A.; Kurauchi, T.; Kamigaito, O.; Kaji, K. *J. Appl. Polym. Sci., Polym. Phys.* **1995**, *33*, 1039.

MA011770D